

NASA/TM-20210015372



Trapped Waves and Screech Tones With Various Rectangular Nozzles

*K.B.M.Q. Zaman and A.F. Fagan
Glenn Research Center, Cleveland, Ohio*

May 2021

NASA STI Program . . . in Profile

Since its founding, NASA has been dedicated to the advancement of aeronautics and space science. The NASA Scientific and Technical Information (STI) Program plays a key part in helping NASA maintain this important role.

The NASA STI Program operates under the auspices of the Agency Chief Information Officer. It collects, organizes, provides for archiving, and disseminates NASA's STI. The NASA STI Program provides access to the NASA Technical Report Server—Registered (NTRS Reg) and NASA Technical Report Server—Public (NTRS) thus providing one of the largest collections of aeronautical and space science STI in the world. Results are published in both non-NASA channels and by NASA in the NASA STI Report Series, which includes the following report types:

- **TECHNICAL PUBLICATION.** Reports of completed research or a major significant phase of research that present the results of NASA programs and include extensive data or theoretical analysis. Includes compilations of significant scientific and technical data and information deemed to be of continuing reference value. NASA counter-part of peer-reviewed formal professional papers, but has less stringent limitations on manuscript length and extent of graphic presentations.
- **TECHNICAL MEMORANDUM.** Scientific and technical findings that are preliminary or of specialized interest, e.g., “quick-release” reports, working papers, and bibliographies that contain minimal annotation. Does not contain extensive analysis.
- **CONTRACTOR REPORT.** Scientific and technical findings by NASA-sponsored contractors and grantees.
- **CONFERENCE PUBLICATION.** Collected papers from scientific and technical conferences, symposia, seminars, or other meetings sponsored or co-sponsored by NASA.
- **SPECIAL PUBLICATION.** Scientific, technical, or historical information from NASA programs, projects, and missions, often concerned with subjects having substantial public interest.
- **TECHNICAL TRANSLATION.** English-language translations of foreign scientific and technical material pertinent to NASA's mission.

For more information about the NASA STI program, see the following:

- Access the NASA STI program home page at <http://www.sti.nasa.gov>
- E-mail your question to help@sti.nasa.gov
- Fax your question to the NASA STI Information Desk at 757-864-6500
- Telephone the NASA STI Information Desk at 757-864-9658
- Write to:
NASA STI Program
Mail Stop 148
NASA Langley Research Center
Hampton, VA 23681-2199

NASA/TM-20210015372



Trapped Waves and Screech Tones With Various Rectangular Nozzles

K.B.M.Q. Zaman and A.F. Fagan
Glenn Research Center, Cleveland, Ohio

National Aeronautics and
Space Administration

Glenn Research Center
Cleveland, Ohio 44135

May 2021

Acknowledgments

This work is supported by NASA's Transformational Tools and Technologies (TTT) and Commercial Supersonic Technologies (CST) Projects.

This report contains preliminary findings,
subject to revision as analysis proceeds.

This work was sponsored by the
Transformative Aeronautics Concepts Program.

Trade names and trademarks are used in this report for identification
only. Their usage does not constitute an official endorsement,
either expressed or implied, by the National Aeronautics and
Space Administration.

Level of Review: This material has been technically reviewed by technical management.

Available from

NASA STI Program
Mail Stop 148
NASA Langley Research Center
Hampton, VA 23681-2199

National Technical Information Service
5285 Port Royal Road
Springfield, VA 22161
703-605-6000

This report is available in electronic form at <http://www.sti.nasa.gov/> and <http://ntrs.nasa.gov/>

Trapped Waves and Screech Tones With Various Rectangular Nozzles

K.B.M.Q. Zaman and A.F. Fagan
National Aeronautics and Space Administration
Glenn Research Center
Cleveland, Ohio 44135

Abstract

This report documents experimental observations made on ‘trapped waves’ occurring with various convergent, rectangular nozzles. Most of the data pertain to three nozzles of aspect ratios (AR) 2, 4 and 8, each having an equivalent diameter of 2.12 in. The trapped waves, manifesting as a series of peaks in the near field pressure fluctuation spectra, are seen with all three nozzles. The number of spectral peaks detected on the major axis is larger than that detected on the minor axis by a factor approximately equal to the AR . These spectral peaks occur in high subsonic conditions and persist into the supersonic regime. Screech tones seem to appear as a continuation of these spectral peaks, i.e., with increasing Mach number it is as if one of these peaks gets amplified and turns into the screech tone. This trend is clearer at smaller AR and gets somewhat obscured at higher AR . Screech frequency variation with Mach number is documented for these and other rectangular nozzles, covering an AR range of 1 to 16. For larger AR (≥ 3), screech frequency is found to scale on the narrow dimension of the nozzle. Screech staging behavior is more pronounced for smaller AR cases. The screech frequency data for the $AR = 1$ (square) case involves multiple stages similar to that of a round nozzle.

Introduction

‘Trapped waves’ in high subsonic jets is a phenomenon uncovered relatively recently by researchers in the academia (Refs. 1 and 2). A brief account of how and why this generated an interest at NASA was given in Reference 3. The current experiments, a continuation of the work reported in Reference 3, were initiated in March of 2020. They were halted due to COVID-19 shutdown and resumed under a limited return-to-work permission. All data presented in the following were obtained in March 2021. The primary objective of the experiment was to document detailed pressure fluctuation spectra for the rectangular nozzles in an effort to aid analytical and numerical studies by colleagues both inhouse as well as at other Institutions. This Technical Memorandum (TM) summarizes key results together with electronic data files.

The data presented are the unsteady pressure fluctuation characteristics near the exits of three rectangular nozzles of aspect ratios 2, 4 and 8, each having the same exit area. With microphones located near the nozzle exit, one on the minor axis and another on the major axis, pressure fluctuation spectra are measured for varying jet Mach number (M_j). Besides documenting the trapped wave characteristics an objective was to study the emergence of screech tones with increasing Mach number and their possible connection to the trapped waves. Another objective was to study just the screech tone frequency variation for a variety of rectangular nozzles. Key results are discussed in the following.

Experimental Facility

The experiments were conducted in an open jet facility at NASA Glenn Research Center (GRC). Compressed air passed through a 30 in. diameter plenum chamber before exhausting through the nozzle into the ambient of the test chamber. A picture of the facility is shown in Figure 1(a) and further descriptions can be found in earlier publications (Refs. 3 to 5). Figure 1 also shows some of the nozzles.

Figure 1(b), (c), and (d) show the ‘R2’, ‘R4’ and ‘R8’ nozzles having aspect ratios of 2, 4 and 8, respectively. These ‘R’ nozzles have been used in previous experiments, (also referred to as ‘NA2Z’, ‘NA4Z’ and ‘NA8Z’ in earlier publications); electronic files on their profiles can be found in, e.g., (Ref. 4). These three nozzles have the same equivalent diameter based on the exit area, $D = 2.12$ in. All dimensions in this document are given in inches. A few other rectangular nozzles are also used to document screech frequency characteristics. This includes a set of rectangular orifices having aspect ratios ranging from 1 to 16; Figure 1(e) shows one of them. These have an equivalent diameter $D = 1$ in. and are denoted as the ‘RO’ cases. Small rectangular nozzles, denoted as ‘R_{sm}’ cases, with $D = 0.58$ in. are also used for screech frequency documentation (Figure 1(f)). The RO and R_{sm} nozzles were originally used for studying spreading characteristics of asymmetric jets (Ref. 5). All nozzles in this study were convergent.

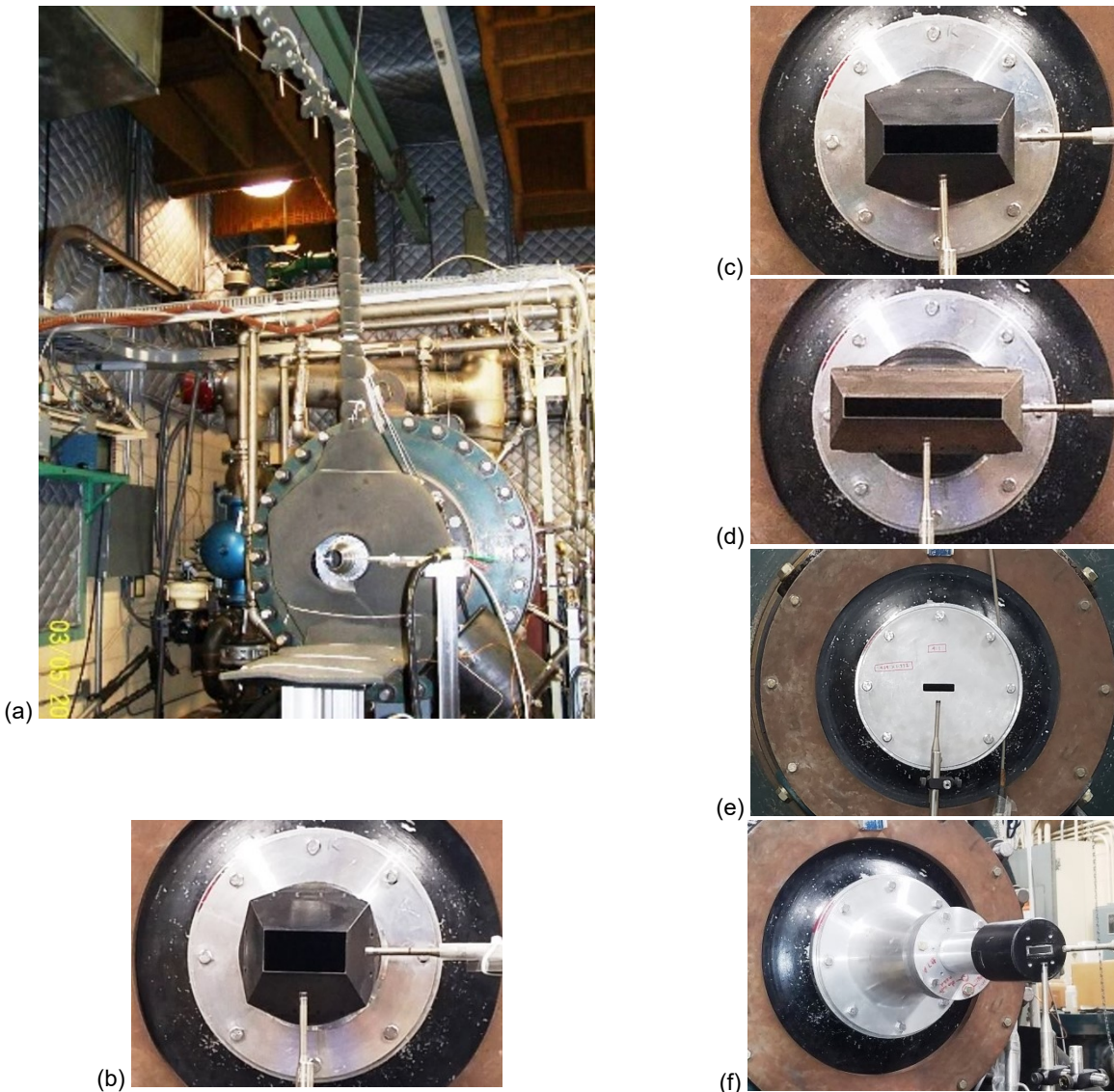


Figure 1.—Facility and nozzle configurations. (a) Jet facility, (b) AR = 2 nozzle (R2), (c) AR = 4 nozzle (R4), (d) AR = 8 nozzle (R8), (e) an orifice nozzle (RO), (f) a small nozzle (R_{sm}). Equivalent diameter $D = 2.12$ in. for the R2, R4, and R8 nozzles in (b) to (d), $D = 1.00$ in. for all RO nozzles (e), and $D = 0.58$ in. for all R_{sm} nozzles (f).

The nozzles were mounted with the long (major) axis placed horizontally. The near field pressure fluctuation spectra on the minor (vertical) axis were measured by a microphone (mic) placed on a fixed stand. A second microphone, mounted on a probe traversing mechanism, was used for measurements on the major (horizontal) axis. Each mic was placed approximately 0.66 in. away from the inner lip of the nozzle and at $x = 0.5$ in. The coordinates x , y and z , with origin at the nozzle exit center, represent the streamwise, horizontal and vertical distances, respectively. (In addition, two other mics were located in the far-field at approximately 25° and 90° relative to the downstream jet axis. These data are not shown in this report but are included in the electronic data files accompanying the TM. Note that with the current setup the usual wrapping of facility surfaces with acoustic absorbent material was not done due to the presence of the near field mics and their support structures. The far-field noise spectra should be considered as qualitative). All mics were of the 1/4-in (B&K 4135) type.

For a given nozzle pressure ratio (NPR) data were acquired from the microphones simultaneously. Data acquisition was done using a National Instruments A/D card and LabVIEW™ software. Spectral analysis was done typically over 0 to 25 kHz with a frequency resolution of 25 Hz, using a data rate of 50 and a 25 kHz low-pass filter. All plots are displayed only to 15 kHz in order to show the trapped wave peaks clearly. For screech frequency data with the $R0$ and the R_{sm} nozzles an analog spectrum analyzer was used to step through NPR and manually record the screech frequency from the spectra.

The ‘jet Mach number’ M_J is used as the independent variable. It is defined based on the plenum pressure, p_0 , and the ambient pressure, p_a , and given by, $M_J = \left(\left(\frac{p_0}{p_a} \right)^{(\gamma-1)/\gamma} - 1 \right)^{1/2}$, where γ is the ratio of specific heats for air, p_0/p_a being NPR. Note that in supersonic conditions, M_J is fictitious and represents the Mach number had the flow expanded fully. All data reported are for cold flows, i.e., with the total temperature the same everywhere as in the ambient.

Results and Discussion

The near field pressure fluctuation spectra, measured on the minor and major axes, are compared in Figure 2(a) and (b) for the $R2$ and the $R8$ nozzles, respectively. These data are for $M_J = 0.91$. Consider the data for the $AR = 2$ ($R2$) case in (a). On the major axis a series of closely spaced spectral peaks occur starting at about 2.5 kHz. These ‘trapped wave spectral peaks’ are also seen on the minor axis, however, they occur less frequently, coinciding approximately with every other peak seen on the major axis. The first (dominant) peak is seen on both axes but only the third and fifth seen on the major axis approximately coincide with the second and third seen on the minor axis. At higher frequencies the amplitudes are small and there is increasing randomness in such matching.

For the $R8$ nozzle (Figure 2(b)) three broad peaks are seen in the minor axis spectra over the range of 0 to 15 kHz. A series of conspicuous but closely spaced peaks can be seen on the major axis especially in the range of 5 to 10 kHz. Note that in the earlier experiment (Ref. 3) only one mic, mounted on the traversing mechanism, was used to obtain the data on the two axis locations successively. In the current experiment two mics are used simultaneously. The mic locations are chosen somewhat farther away in the present experiment, (0.66 in. from the lip as opposed to 0.33 in. earlier), to minimize any disturbance because of the presence of the two mics. In Figure 2(b), roughly eight peaks in the major axis spectra can be counted within the span of a broad peak seen on the minor axis. With similar data at various M_J and also for the $R4$ nozzle it is inferred that the ratio of the number of peaks seen on the major axis and that on the minor axis approximately equals the aspect ratio of the nozzle. Thus, it appears as if a lateral resonance in the major axis direction, whose wavelength is dictated by the major dimension, is detected on the minor axis location. On the other hand, a resonance with wavelength dictated by the minor dimension is detected on the major axis location.

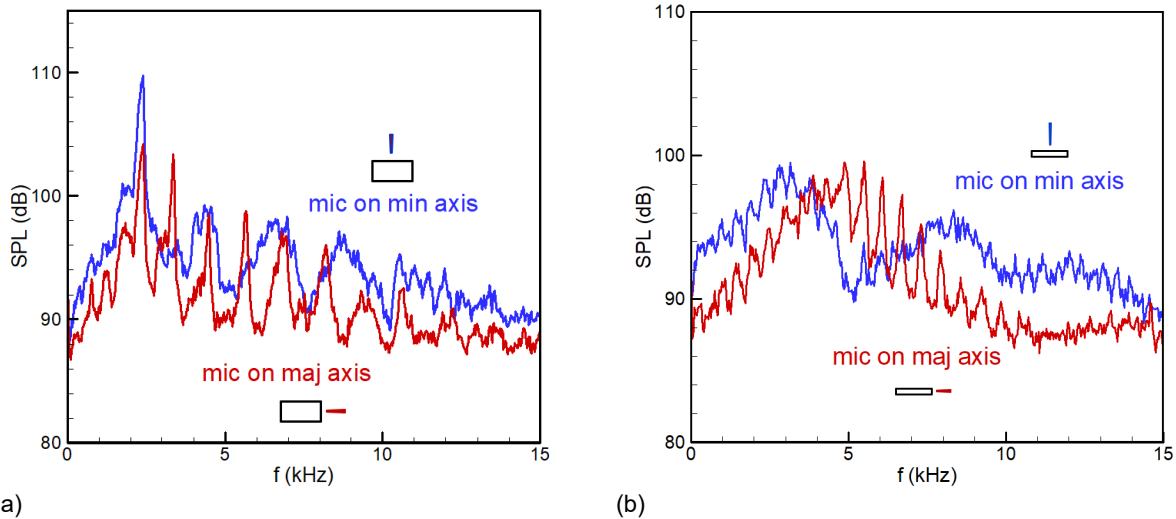


Figure 2.—Pressure fluctuation spectra at $x = 0.5$ in., $M_J = 0.91$, with mic on minor axis (blue line) and mic on major axis (red line). (a) data for $R2$ nozzle, (b) data for $R8$ nozzle; microphone is placed 0.66 in. from the nozzle lip.

The primary objective of the experiment was to document detailed near field pressure fluctuation characteristics for the $R2$, $R4$ and $R8$ nozzles, in order to aid analytical and numerical efforts by colleagues. While Figure 2 is used to introduce the trapped wave spectral characteristics, detailed spectral evolution with varying M_J are shown in the following. Figure 3 shows such data for the $R2$ nozzle in a ‘waterfall’ format. For clarity the results are divided into two plots for lower and higher Mach number regimes, shown in the bottom and top rows, respectively. Data for minor axis location are in the left column while those for major axis location are in the right column. The value of M_J is indicated on the right of each spectral trace. A visual perspective on the evolution of the trapped wave spectral peaks can be obtained from the lower M_J data in the bottom row.

Consider the minor axis data on the lower left of Figure 3. The trapped wave ‘fundamental’ peak (dominant peak at the lowest frequency) is barely visible at the lowest M_J . With increasing M_J it becomes prominent and persists into the supersonic regime, while its frequency continuously decreases. Noticeable higher frequency peaks appear around $M_J = 0.81$. Here, the higher frequency peaks appear to be (integral) harmonics of the fundamental. Note that for a round nozzle multiple trapped wave peaks were also observed where the higher frequency peaks were not integral harmonics; they appeared to be $5/3$, $7/3$... multiples of the fundamental (Ref. 3).

The transition of the spectral peaks into screech can also be seen from the minor axis data. At about $M_J = 1.14$, the second trapped wave peak (first harmonic) suddenly gets amplified into a sharp spike with accompanying screech tone (in this instance at 3.64 kHz). The plot in the upper row (Figure 3 left) captures subsequent evolution of the screech tone. Screech frequency continues to decrease with increasing M_J . At high M_J , the harmonic relationship with the trapped wave fundamental is lost. At $M_J = 1.14$, the fundamental and screech components occur at 1.82 and 3.64 kHz, respectively (harmonics). At $M_J = 1.28$, for example, these two peaks occur at 1.63 and 2.81 kHz, respectively (not harmonics).

The data for the major axis location on the right of Figure 3 show a similar spectral evolution. The fundamental trapped wave peak remains the same as seen on the minor axis. However, the number of peaks is more. A comparison at a given M_J , especially at subsonic conditions, shows that for each pair of adjacent peaks on the minor axis there is a third in the middle of the corresponding data on the major axis.

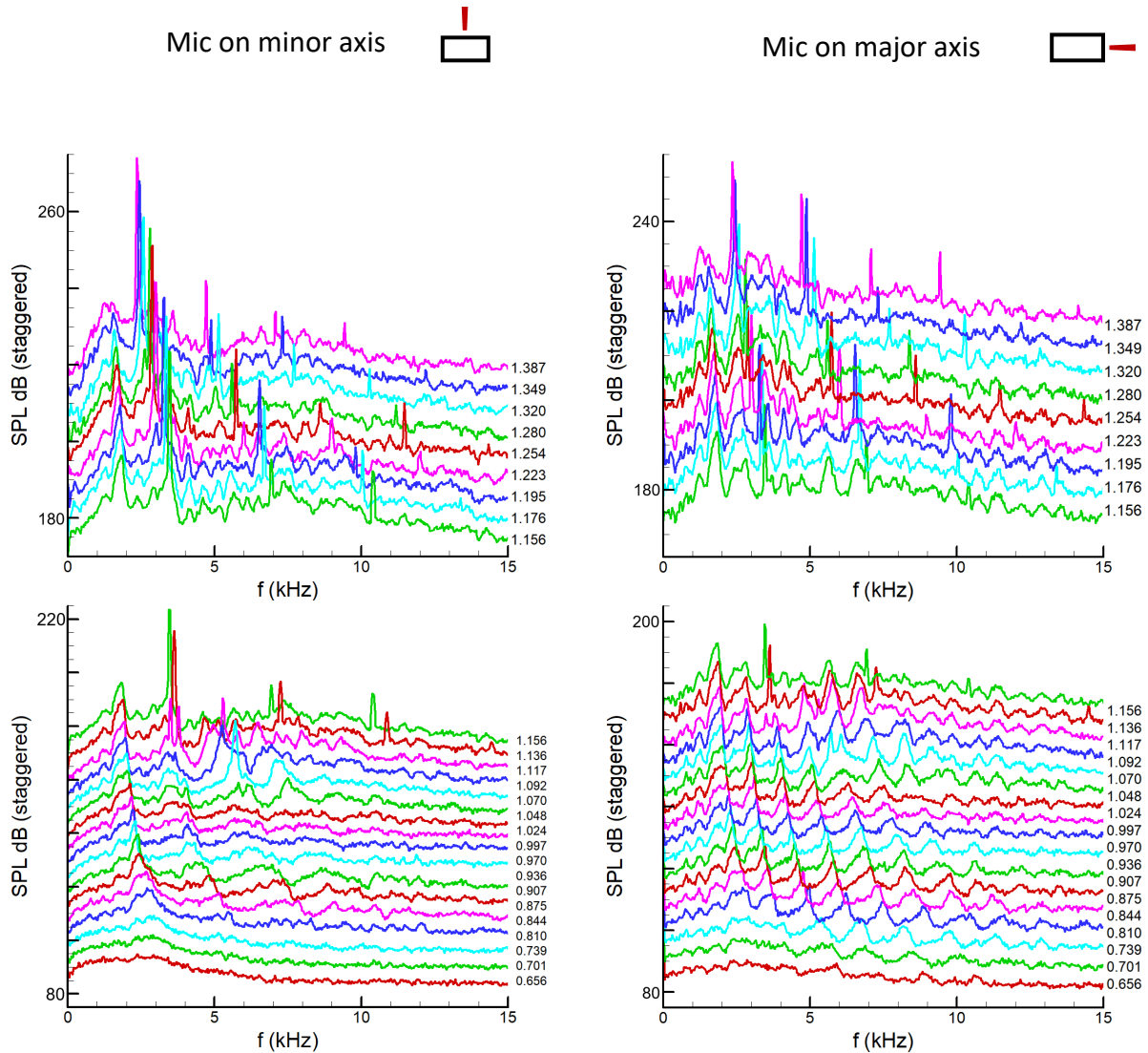


Figure 3.—Near field pressure fluctuation spectra for the $AR = 2$ nozzle ($R2$). Left column for mic on minor axis, right column for mic on major axis. Bottom row for lower M_J -range, top row for higher M_J -range. In each figure successive traces are staggered by 5 dB (minor tick spacing on the ordinate axis); ordinate scale pertains to lowest trace in the figure on bottom. M_J for each trace indicated on the side.

Spectral evolution data for the $R4$ nozzle are similarly shown in Figure 4. Here, the trends in the evolution are somewhat obscure. The trapped wave fundamental on the minor axis (left column) becomes clear at a somewhat higher M_J (approximately 0.9). As with the $R2$ nozzle, the fundamental persists all the way to the highest M_J ($= 1.39$) covered in the experiment. However, the higher harmonics of the fundamental are not quite clear. Screech ensues at $M_J = 1.05$ at a relatively high frequency, appearing to coincide with the 2nd harmonic of the fundamental. At slightly higher M_J (1.12) it jumps to a lower frequency appearing to be near the first harmonic. With increasing M_J , the screech frequency decreases at a rate faster than that of the fundamental. In general, the cluster of screech peaks appear to occur near the first harmonic. These trends will be scrutinized further in the future possibly with additional data. On the right of Figure 4, at the major axis location, the trapped wave peaks are clearer in the subsonic regime. A band of those peaks appear at higher frequencies and this band moves to the left with increasing M_J until screech appears at $M_J = 1.12$.

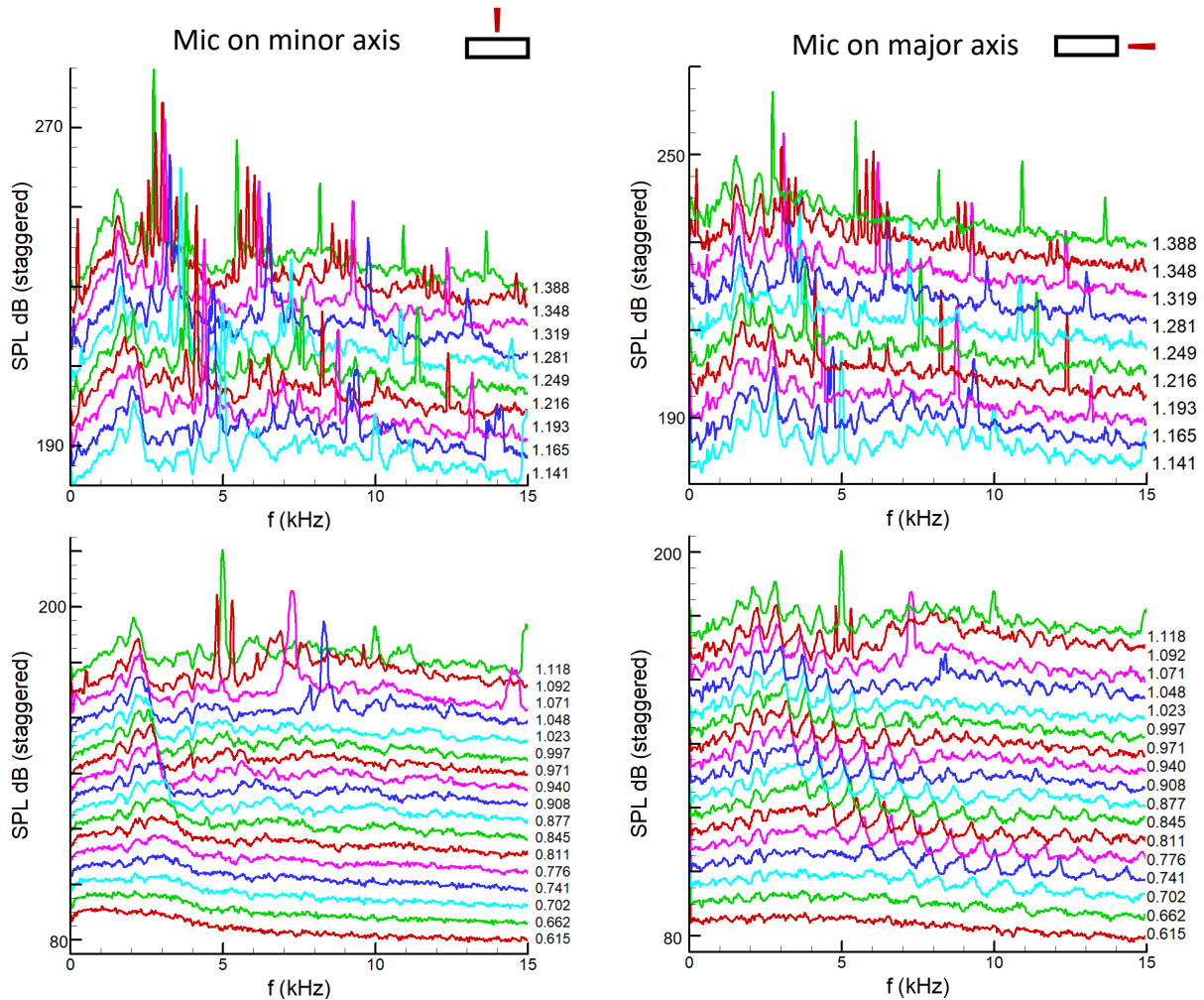


Figure 4.—Near field pressure fluctuation spectra for the $AR = 4$ nozzle ($R4$), shown similarly as in Figure 3.

Corresponding data for the $R8$ case are shown in Figure 5. Similar observations can be made as with the $R4$ data in Figure 4. We note that for both $R4$ and $R8$ cases, screech appears to start around $M_J = 1.05$ occurring near the second harmonic of the fundamental. This could be an early screech stage. Subsequently, the frequency of the screech tone drops to coincide with the first harmonic. Overall, the screech peaks are seen clustered around the first harmonic of the trapped wave fundamental for all three nozzles. Note that a similar observation was made for round nozzles in Reference 3; with increasing M_J it was as if one of the trapped wave peaks abruptly increased in amplitude to turn into the audible screech tone. However, a clear connection between screech and the trapped waves remains to be understood.

Time series microphone data were recorded for limited Mach numbers with the R nozzles. Coherence between the signals from the major and the minor axis microphones was investigated. The coherence data for the $R2$, $R4$ and $R8$ nozzles are shown in Figure 6 for $M_J = 0.91$, as examples. The three plots are for the three nozzles, coherence being shown by the black curves with ordinate on the right. Corresponding spectral data are shown at the bottom of each plot with ordinate on the left (red and blue curves) for reference. It is apparent that the coherence at the trapped wave fundamental is high for the $R2$ nozzle. Such coherence is progressively weaker with increasing aspect ratio. Of course, when screech occurs the coherence is nearly unity at the tone frequency for all nozzles (these data are not shown for brevity). In the following, the screech frequency characteristics are studied in detail.

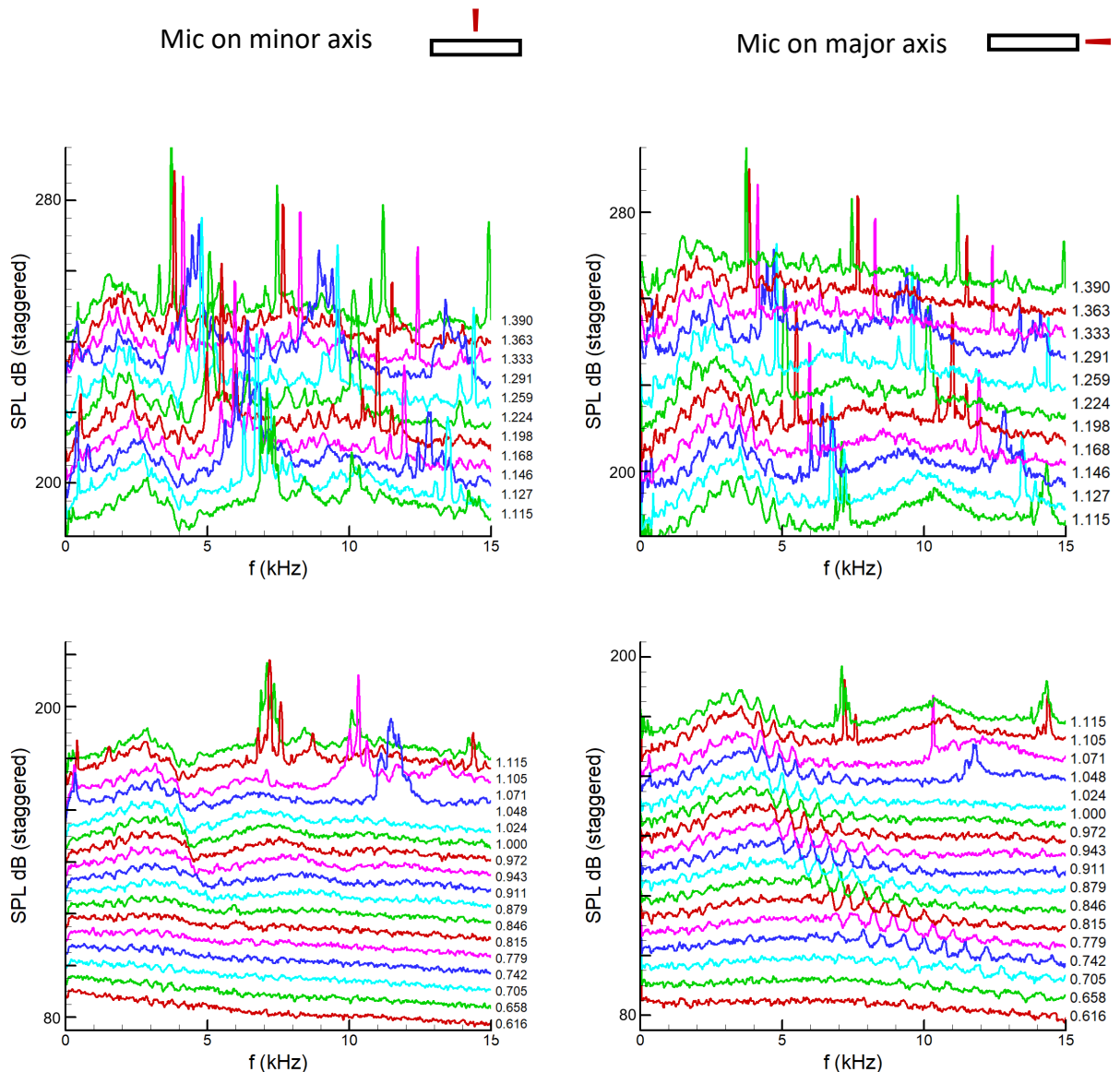


Figure 5.—Near field pressure fluctuation spectra for the $AR = 8$ nozzle ($R8$), shown similarly as in Figure 3.

In addition to documenting screech frequency variation from the data shown in Figure 3 to Figure 5, further data were acquired with other rectangular nozzle configurations. This effort was prompted partly by a confusion in rectangular nozzle screech data in the literature (Prof. Mo Samimy, private communication; see also (Ref. 6)). Part of the confusion arose because in an earlier work with small nozzles (Ref. 5), $c_a * M_J$, instead of U_J , was used as velocity scale to calculate Strouhal number; here c_a is speed of sound in the ambient and U_J is the ‘fully expanded velocity’ (ideal velocity had the flow expanded fully for a given NPR). The data in Reference 6, as in many other related work, are presented as Strouhal number based on the equivalent diameter (D) and U_J . This format of nondimensionalization is examined in the following.

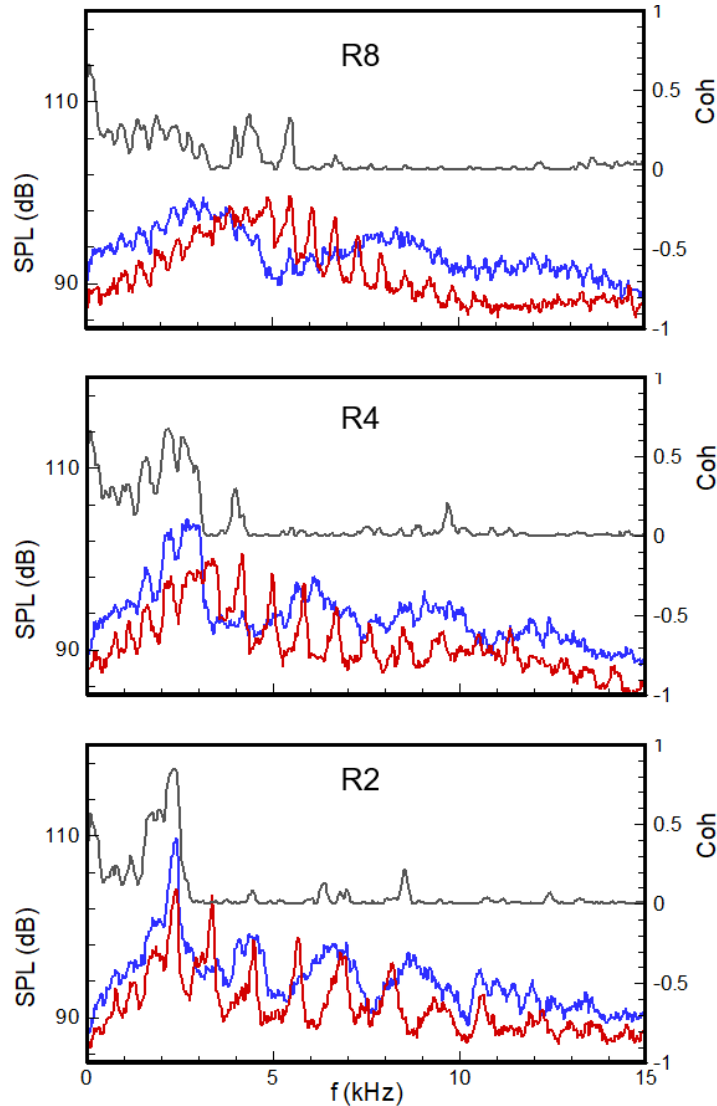


Figure 6.—Coherence between signals from microphones on the major and minor axes. Data for the *R2*, *R4* and *R8* nozzles shown, as indicated. In each figure, the spectra from minor axis (blue) and major axis (red) are shown at the bottom.

First, the screech data for the *R2*, *R4* and *R8* nozzles are shown in Figure 7. Note that the two high frequency data for the *R4* and *R8* nozzles at $M_J = 1.07$ and 1.11 (Figure 4 and Figure 5) are ignored so that the trends for the three data sets could be shown with sufficient ordinate resolution. As expected, for each nozzle the Strouhal number of screech decreases with increasing M_J . It also becomes clear that the aspect ratio factors into the data trends; fD/U_J at a given M_J is increasingly larger with increasing AR . Figure 7 also includes screech data taken with the orifice nozzles (Figure 1(e)) of same AR values (2, 4, and 8). Screech ensues at a lower M_J with the *R* nozzles compared to the data for the *RO* nozzles. Note that the data could be obtained with the *R* nozzles only up to about $M_J = 1.4$. This is because with these bigger nozzles ($D = 2.12$ in.) the flow rate becomes so large as to cause excessive recirculation flow in the confined test cell. With the smaller *RO* nozzles ($D = 1$ in.) this was not a problem and the data could be taken at higher M_J values. It is seen that for a given AR the nondimensional frequencies agree well between the two sets of nozzles. With aspect ratio 2, two stages of screech could be observed with the *RO* nozzle, the jump occurring around $M_J = 1.4$. The stage at higher M_J is missed with the *R* nozzles due to facility constraints mentioned above.

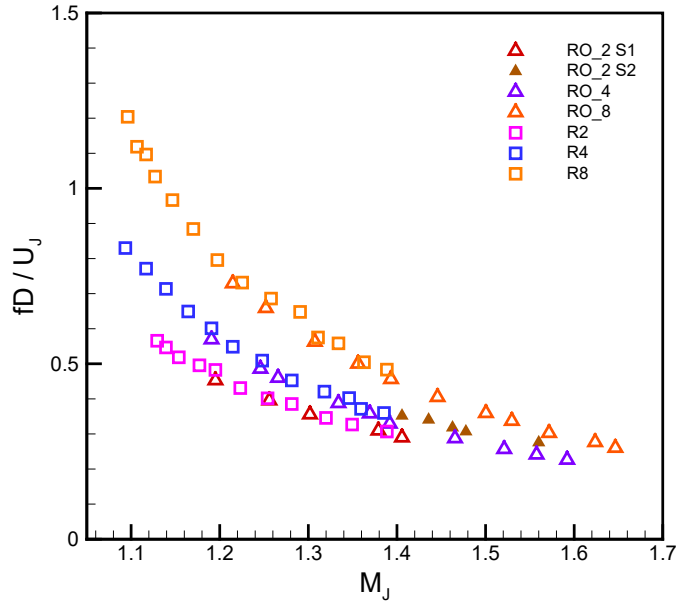


Figure 7.—Screech data for R2, R4 and R8 nozzles compared to data from orifice cases having corresponding aspect ratios.

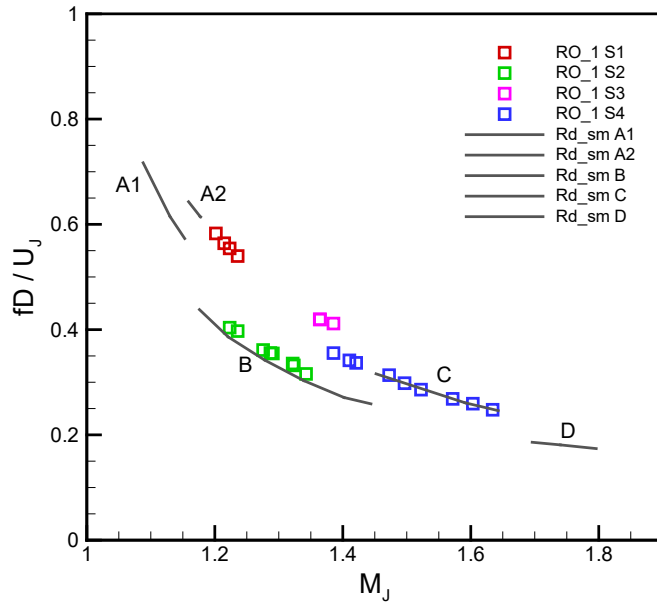


Figure 8.—Screech data from square orifice case compared to round nozzle data.

In order to complete an understanding of the effect of AR , further data were taken with various RO nozzles. Figure 8 shows data for an $AR = 1$ (square, RO_1) case, compared to circular nozzle (Rd_sm) data. The latter data shown by the solid lines are reproduced from Reference 5. The well-known screech stages for the circular case are indicated in the figure. It is apparent that the square nozzle behaves quite similarly involving multiple stages, some of the stages seemingly coinciding with the circular jet data. Further data with larger AR cases are shown in the following.

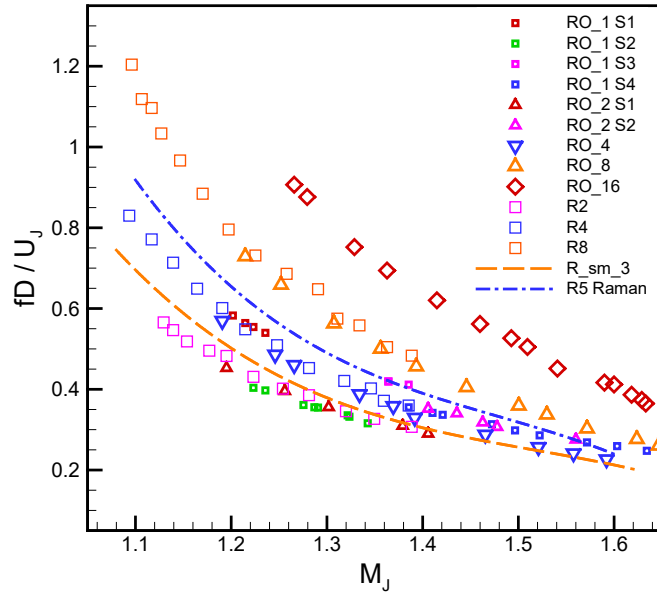


Figure 9.—Screech data for various rectangular nozzles.

Data for all rectangular cases are shown in Figure 9. This includes data from a *RO* nozzle with $AR = 16$, data for a small $AR = 3$ nozzle (*R_sm_3*) reproduced from Reference 5, and another set of data for an $AR = 5$ nozzle obtained in the same jet facility from Reference 7. While the square nozzle involves multiple stages and the $AR = 2$ case involves two stages, the rest of the data involve just one stage within the M_J range covered. Note that the data from References 5 and 7 are reproduced by digitization of the published graphs (and converted appropriately). Average curves through the data of these two cases are shown by the lines; (the slightly downward bends of these curves on the far right are likely to be artifacts of curve fitting).

It is worth mentioning that the data with the $AR = 5$ case reproduced when obtained in a different facility (Ref. 8). Also, in the present experiments, brief checks were made for a small $AR = 3$ nozzle (same as used in Reference 5) and the data were found to repeat well. (There was a stage jump noted in Reference 5) around $M_J = 1.65$, the line in Figure 9 represents the first stage). We note here that in Reference 6 the authors report a detailed study of twin rectangular jet interactions using $AR = 2$ convergent-divergent (C-D) nozzles each having a design Mach number of 1.5. Interesting observations were made such as differences in the coupling modes that depended on whether the jets were overexpanded or underexpanded. In connection with this work, they compiled single rectangular jet screech data from several sources. These data were for the AR range of 2 to 5 and the authors noted a good collapse of the data when plotted in the coordinates of Figure 9. However, several data sets, including their own with $AR = 2$ were from C-D nozzles. It remains unclear if the screech frequencies are also affected by the design Mach number of the C-D nozzle as well as the flow regime. All nozzles in Figure 9 are convergent and the flows are underexpanded.

It is clear in Figure 9 that there is a systematic trend based on AR . The trend suggests that the narrow dimension of a rectangular nozzle dictates the screech frequency, at least for some of the cases. This is examined in Figure 10 where the same data of Figure 9 are replotted as Strouhal number based on the narrow dimension (h) and U_J . The ordinate scale is kept the same as in Figure 9 so that the relative collapse of the data is displayed. Apart from the $AR = 1$ and 2 cases, all other data involving aspect ratios, 3, 4, 5, 8, and 16 are all clustered into one curve. Thus, for aspect ratios greater than 3, the narrow dimension is the right length scale dictating the screech frequency. When the aspect ratio is smaller than 3 the flow does not behave as ‘two-dimensional’ and the data trend deviates; there are 3-D effects and the data are also characterized by multiple screech stages.

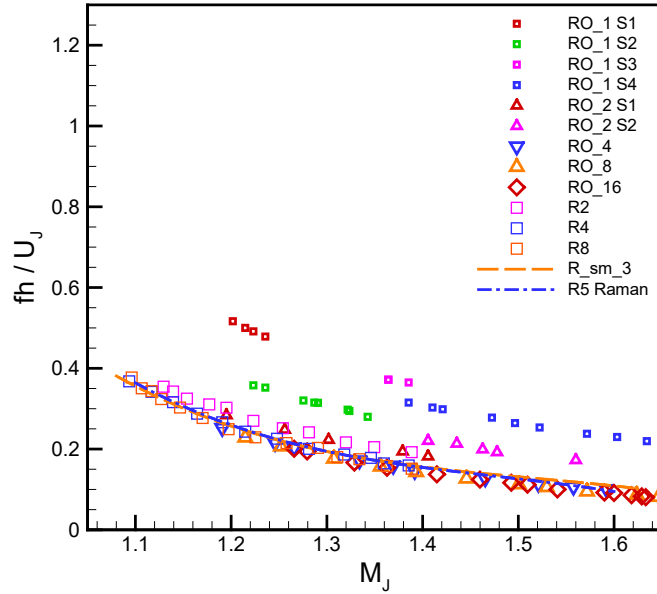


Figure 10.—Same data from Figure 9 plotted as a function of Strouhal number based on the narrow dimension (h).

Supplemental data files corresponding to the spectra in Figure 3 to Figure 5 are available with the electronic version of this TM at www.sti.nasa.gov. Each file has data from four microphones recorded in block format. The third and fourth blocks are the data from the minor axis and major axis locations, respectively. Microphone location, M_j and OASPL values are indicated in the header of each block (zone). (Data in the first two blocks are far-field data, from approximately 25° and 90° polar locations, acquired simultaneously. Referring to the discussion in the “Experimental facility” section, these should be considered as qualitative.)

Conclusions

Near field pressure fluctuations for three rectangular nozzles with aspect ratios of 2, 4 and 8 are explored experimentally. With all three cases the trapped wave spectral peaks are observed. The frequencies of the peaks depend on the observation location. More tightly packed spectral peaks occur on the short edge (i.e., on the major axis) while the peaks are dispersed on the long edge (i.e., on the minor axis). The ratio of the number of peaks on the short and long edge is found to be approximately equal to the aspect ratio of the nozzle. These spectral peaks persist into the supersonic flow regime. Screech tones seem to appear as a continuation of these spectral peaks; with increasing Mach number the first harmonic of the trapped wave fundamental appears to get amplified and turn into the screech tone. This trend is clearer for the $AR = 2$ case but gets somewhat obscured at higher AR . Screech tone frequency variation with Mach number is documented for these as well as other rectangular nozzles, covering AR from 1 to 16. For $AR \geq 3$, screech frequency is found to scale on the narrow dimension of the nozzle; all data when plotted as Strouhal number based on the narrow dimension versus jet Mach number are found to collapse on a single curve. Screech staging behavior is found to be more pronounced for smaller AR cases. The screech frequency data for the $AR = 1$ (square) case involves multiple stages similar to that of a round nozzle.

References

1. Towne, A., Cavalieri, A.V.G., Jordan, P. Colonius, T., Schmidt, O., Jaunet, V. and Brès, G.A., “Acoustic resonance in the potential core of subsonic jets,” *J. Fluid Mech.*, vol. 825, pp. 1113–1152, 2017.
2. Schmidt, O.T., Towne, A., Colonius, T., Cavalieri, A.V.G., Jordan, P. and Bres, G.A., “Wavepackets and trapped acoustic modes in a turbulent jet: coherent structure education and global stability,” *J. Fluid Mech.* 825, 1153–1181, 2017.
3. Zaman, K.B.M.Q. and Fagan, A.F., 2020, “Pressure Fluctuations due to ‘Trapped Waves’ in the Initial Region of High-speed Jets,” *AIAA Paper 2020-2523*, Aviation Forum, June 15–19, 2020. (see also, “Near-exit pressure fluctuations in jets from circular and rectangular nozzles,” NASA/TM—2019-220383, November 2019.)
4. Zaman, K.B.M.Q., “Flow Field Surveys For Rectangular Nozzles,” NASA/TM—2012-217410, April, 2012.
5. Zaman, K.B.M.Q., “Spreading characteristics of compressible jets from nozzles of various geometries,” *J. Fluid Mech.*, 383, pp. 197–228, 1999.
6. Esfahani, A., Webb, N. and Samimy, M., “Coupling Modes in Supersonic Twin Rectangular Jets,” *AIAA Paper 2021-1292*, SciTech Forum, January 2021.
7. Raman, G. “Cessation of Screech in Underexpanded Jets,” *J. Fluid Mech.*, vol. 336, pp. 69–90, 1997.
8. Panda, J., Raman, G., and Zaman, K., “Underexpanded Screeching Jets from Circular, Rectangular and Elliptic Nozzles,” *AIAA Paper 97-1623*, 3rd AIAA/CEAS Aeroacoustics Conference, Atlanta, Georgia, May 12–14, 1997.

